https://www.imavs.org/pdf/imav.2010.1

A Tilt-Body Fixed-wing Micro Air Vehicle for Autonomous Transition Flight

Ryan Carr[1]
l'Office National d'Etudes et Recherches Aérospatiales (ONERA), Toulouse, France

Jean Marc Moschetta[2] and Gaurang Mehta[3]
Institut Supérieur de l'Aéronautique et de l'Espace(ISAE), Toulouse, France

Chinnapat Thipyopas[4]
Kasetsart University, Bangkok, Thailand

The increasingly complex urban battlefield calls for Micro Air Vehicles (MAV) capable of performing missions combining the speed of horizontal flight and the precision of vertical flight. Towards this end, an aircraft has been developed at ISAE to perform both these missions. The MAVion is a dual motor tilt-body aircraft that has already been demonstrated in horizontal flight. The present effort focuses on modifying the horizontal version for vertical flight. The modifications include replacement of the autopilot hardware, redesign of the control software to make use of the quaternion rotations, and developing composite fabrication of the structure for improved robustness to hard landings. Attempts have also been made to model the complex aerodynamics of propeller slipstream impingement on a wing during transition between vertical and horizontal flight modes. The vertical flight version of the aircraft will be demonstrated during the International MAV competition held in Braunschweig, Germany, July 2010.

I. Introduction

Modern urban reconnaissance missions dictate the need for a MAV platform capable of performing a complex mission: rapid and efficient ingress to a target location followed by slow loiter for quality image capture. This mission must be performed despite the presence of typical urban obstacles, possible lack of GPS, and erratic wind-gusting. This may be achieved using a tilt-body fixed-wing vehicle, which combines the speed, range, and gust-hardiness of a fixed wing with the loiter and precision capability of a rotorcraft vehicle.

At the 2009 International MAV competition held in Pensacola, Florida, a team of students from l'Institut Superieur de l'Aeronautique et de l'Espace (ISAE) demonstrated a new aircraft called the MAVion, winning first place in the Precise Navigation competition. Work on the MAVion airframe has continued, with the challenge of developing a platform capable of performing a smooth transition between horizontal and vertical flight modes. The present effort is focused on the vertical flight portion of this goal.

This capability has been demonstrated previously by larger aircraft as early as the 1950's with the Convair XFY-1 and Lockheed XFV. Although the concept was demonstrated, the projects were abandoned partly due to the difficulty of training pilots to land the aircraft[1]. With the advent of UAV's the skill of the pilot is no longer a limitation, and autopilots are relatively easy and inexpensive to develop. This has caused a resurgence in the tilt body concept in industry, academia, and defence in recent years[2,3,4].

One notable example is the *T-Wing* developed by Stone[5], who has produced a large amount of research including trajectory optimization, control design, 6 DOF simulation, and computational modelling of wing-propeller interactions for his VTOL aircraft.

---

[1] Aeronautical Research Engineer, ONERA/DCSD, 31055 Toulouse cedex 4, France, ryan.carr@onera.fr
[2] Professor, ISAE/DAEP, 31055 Toulouse cedex 4, France, Jean-Marc.Moschetta@isae.fr
[3] Student, ISAE/DAEP, Toulouse cedex 4, France, gaurang.mehta@isea.fr
[4] Associate Professor, Dept. of Aerospace Engineering, Kasetsart University, Bangkok, Thailand chinnapat.t@ku.ac.th

http://www.imavs.org/

http://www.imavs.org/

An interesting tailsitter controller was recently developed and demonstrated by Knoebel[6]. His backstepping controller based exclusively on quaternion rotations, used least-squares parameter estimates of a simplified aerodynamic model to adapt to the changing aerodynamics of transition flight. Successful flight testing validated the utility of the adaptive controller. The PD quaternion controller developed for the present work is partly based on this promising research.

The method of calculating propeller interactions as applied to the *Vertigo* project reported by Poinsot[7] has been applied while modelling the aerodynamics of transition flight. This method, which will be described in detail, allows a simple estimate of the complicated aerodynamics involved. A 6 DOF simulator has also been developed based on this model. Pictures of the three aircraft described above are given in Figure 1.

Figure 1. From left to right: T-Wing (Stone), Tail-Sitter (Knoebel), Vertigo (Poinsot)

As mentioned above, the MAVion has already been demonstrated as a capable platform in horizontal flight. An image of the MAVion as featured at IMAV 2009 is given in Figure 2. The current work seeks to adapt this successful design to perform vertical flights, and more challenging, a smooth transition between the two modes.

Figure 2. The MAVion competing in IMAV 2009

The previous version of the MAVion was outfitted with a PAPARAZZI autopilot[8], a widely used open-source autopilot developed at the *Ecole Nationale de l'Aviation Civile* (ENAC). This version of the autopilot was outfitted with IR horizon detection sensors to determine attitude in flight. This method would obviously not be applicable to low altitude vertical flight. It was decided to move to a new autopilot system, recently developed in-house at the *Institut Supérieur de l'Aéronautique et de l'Espace* (ISAE). Because the new autopilot system was heavier than the previous, and the motors on the horizontal version are too small to support extended vertical flights, some modifications were made to the original design of the MAVion.

II. Aircraft Design

Whenever possible, the original design of the MAVion was maintained. The MAVion concept is based on several simple design features which improve mission performance. The counter-rotating propellers cancel torque, eliminating the need for a drag-increasing bias in the ailerons. The propellers are mounted tandem, which differently from coaxial designs, allows for a MAV with a greater aspect ratio, improving horizontal flight efficiency. The direction of rotation of the propellers is chosen to generate swirl which counters wingtip vortices, effectively reversing the phenomenon. Mounting the motors in tractor configuration provides a blowing effect which maintains attached flow at higher angles of attack by inserting energy into the flow. Finally, by tilting the entire body instead of just motors or wings, the overall structure is simplified while still allowing for complex, multi-task missions. All of these basic design concepts were maintained with the vertical version of the MAVion.

There were some specific component changes, however. The former motors were estimated to produce roughly 2.5 N of static force at maximum throttle. Although this may be enough to hover the horizontal version without

change, a sustained hover would very likely overheat the 10 gram motors. In addition, it was necessary to compensate for the increased weight of the autopilot system. Thus the size of the motors and the wingspan was increased. In the end, the motor size was nearly doubled, while the total weight increased by 28%. In order to maintain a low wing-loading and stall velocity in horizontal flight, the wingspan was increased by 17%, along with a proportional adjustment to all other structural dimensions.

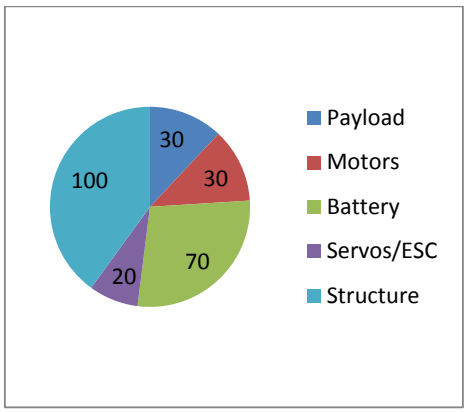

Figure 3. Mass breakdown of horizontal MAVion. Total mass: 250 grams

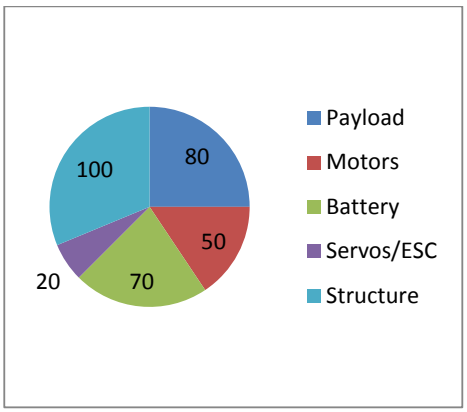

Figure 4. Mass breakdown of vertical MAVion. Total mass: 310 grams

III. Composite Fabrication

The original version of the MAVion was constructed from Expanded Polypropylene (EPP) with a film covering. Although EPP wings, fuselages, and fins were cut using a CNC foamcutter, large variations were seen from one version to the next, while fabrication of complex geometries such as fairings and fillets was very difficult. To improve the precision of construction, moulds were created to permit fabrication of the aircraft from composite materials. First, a3D CATIA model of the MAVion was created. A fuselage was designed to house the IMU, autopilot board, and battery. Motor fairings and filleting were added to reduce drag. A vertical stabilizer with a NACA 0060 airfoil was designed to replace the previous flat plate fin. An image of the final design is shown in Figure 5.

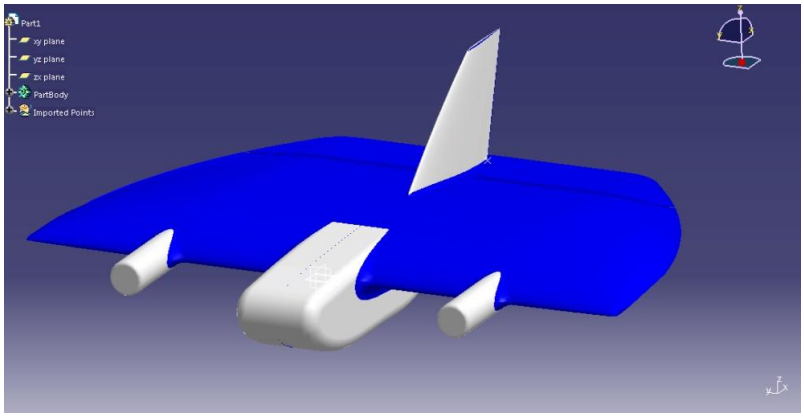

Figure 5. CATIA drawing of MAVion. Used to produce molds for composite aircraft.

This geometry was used to machine moulds which could then be used to lay up composite versions of the aircraft. One advantage of using composites is that the structure can easily be tailored to suit the application. For example, a very rigid but heavy version of the MAVion was created for wind-tunnel testing using two thick layers of fibre-glass. The final flight version of the aircraft is composed of a thin layer of stiff, light carbon on

http://www.imavs.org/

the wings, with two thin layers of less fragile fibre-glass for the fuselage. All versions contain an EPP core that serves for component placement and dampens shock during crashes.

The fabrication process for one aircraft requires roughly 3 days of labour, including mould preparation, composite curing, and component installation. The process is here outlined in brief to document for future fabrication.

A. Polish and wax moulds to ensure proper release of composite material. Thorough sandpaper polishing should be followed by liquid polish to ensure a completely smooth surface. Mold release agent is then applied, followed by several layers of wax. Each layer of wax is allowed to completely dry before rubbing off the excess.

B. Composite materials are selected and cut to size. Care should be taken to ensure the material piece is sufficiently large to completely cover the surface of the mold. For complex corners, the material may be cut and folded, but this should be avoided as it weakens the structure. Small pieces of extra material may be added to areas which require extra stiffness. For portions requiring flexibility (such as the elevon joints), a layer of Kevlar may be used. After the epoxy cures, the Kevlar can be bent to break the cured epoxy, providing a flexible yet durable joint.

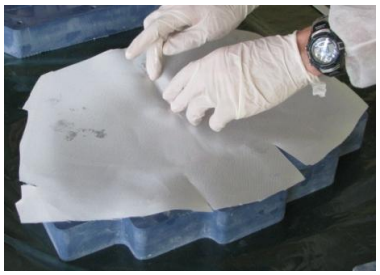

C. Epoxy is prepared in proportions as indicated. Gloves should be worn when handling epoxy. Epoxy-safe paint may be applied to the surface of mold directly. While the paint is still wet, the chosen material (laminate) is carefully placed over the surface of the mold, and covered in a thin layer of epoxy. Once all layers are in place, counter-molds may be used to ensure the laminate maintains contact with complex geometries, such as the fuselage and fairings.

D. Peel ply, perforated release films, bleeder and breather cloths are added above the laminate material. The molds and materials are placed into a vacuum bag, a vacuum port is attached, the vacuum bag is sealed, and pressure is reduced as low as possible. Although placing the bag into an oven may accelerate the curing process, it is not strictly necessary. A small amount of epoxy mixture can be set aside to check progress of the cure.

E. After epoxy has fully cured (usually overnight or a weekend), the vacuum bag, breathers, bleeder cloth, perforated films and peel ply may be removed. Carefully lift the cured laminate from the mold. Compressed air may be used to push stuck areas. Avoid using hard materials to help release the laminate, as this will likely scratch the mold, requiring repolishing before future use. Carefully cut excess laminate with the appropriate tool in a properly vented area. Care should be taken with carbon as it can produce dust which can irritate the skin or lungs if inhaled.

F. Cut EPP core using CNC foam cutter. Carve slots in foam for autopilot board, servos, electronic speed controllers (ESC), and tracks for the wiring. Install switch in fuselage. Cut hatch for battery in fuselage.

http://www.imavs.org/

http://www.imavs.org/

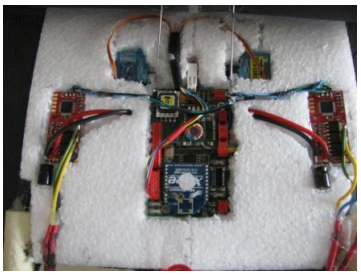

Cut slots in elevons 10 cm to either side of the root to permit movement of the control surfaces. Cut exit slots for control pushrods in the upper surface, allowing enough room for complete movement of servo arms. Install control horns in elevons near the rear of the surface to increase maximum throw. Cut and install cylindrical polystyrene inserts inside the motor fairings. These are pierced down the axis to allow passage of a 6 mm diameter carbon shaft upon which the motors are attached. The shaft is allowed to freely rotate within the foam, as is attached to the lower surface with a light layer of epoxy. This is to dampen shock to the motor mount in the event of a crash. Pierce holes for antennae. Mount ultrasonic rangefinder to lower surface between control surfaces. The upper and lower surfaces may be attached with epoxy, or simply left open and taped for easy access to components.

IV. Motor-Propeller Selection

The choice of propulsion system for an aircraft in vertical flight mode is critically important, as it directly provides all the lift, and it is also the part of the system most likely to fail if not designed properly. Although simulation tools have been used to determine the proper propulsion system for the MAVion, it is always necessary to fully test any choice experimentally. The simulation tool used as a first look at motor and propeller choice was QPROP, created by Mark Drela[9], author of various other useful tools for small aircraft such as XFOIL and AVL. QPROP uses a blade-element vortex method which can be used even for the static case, such as would be encountered for hover. Lift on propeller blades is modelled as linear with stall limits, while drag is calculated as a quadratic function of the lift coefficient, with power scaling by the Reynolds number. The user must supply the above aerodynamic parameters (easily obtainable using XFOIL), as well as geometric parameters describing the propeller. Motors are modelled as brushed DC, using standard electric motor parameters such as the RPM/volt constant Kv, the motor resistance R (Ohms), and the no load current I_0 (Amps).

To begin, a propeller/motor combination was chosen that was hoped would provide sufficient thrust to hover the 300 gram aircraft. Parameters used in QPROP are given below:

Motor	Kv	R (Ohms)	I_0 (Amps)
XC2205	2200	0.2	0.8

Propeller	Radius	CL0	CL_a	CD0	CD2u	CD2l	CLCD0	REref	REexp
GWS 5x3x3	0.127	0.1	2.5	-0.014	0.4	0.1	0.4	70000	-0.3

This motor/propeller combination was modelled in QPROP, and curves of RPM vs thrust and current draw were produced. The simulation seemed to indicate that the chosen combination was sufficient, so experimental testing was begun to provide further data. Testing was performed on a test-bench developed at the propulsion laboratory of ISAE.

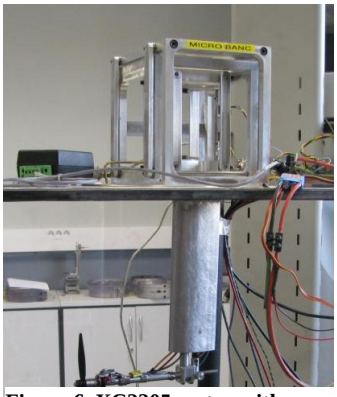

Figure 6. XC2205 motor with GWS5x3x3 propeller mounted on the *MicroBanc* test bench at ISAE.

Experimental thrust and current data were collected for the motor/prop combination reported above. Thrust data has been compared with the data generated using QPROP in Figure 7. As can be seen, the thrust data compares very well. This is somewhat surprising considering that the QPROP data was generated before any testing was performed. The current data is not a good match, however. This is likely due to multiple factors. First, the motor parameters used in the simulation need to be adjusted. Also, the model used in the simulation probably does not predict the amount of heating developed in the motors during the experiments. This heating

decreases motor efficiency, increasing current draw, and further heating the motor.

The experimental current data shows that a low current consumption is expected up until around a175 RPS, at which point the current shoots up dramatically with little gain in rotation speed. The motors are rated to be able to operate at 6 amps for only short bursts. However, with the propeller and motor combination selected, that only turns the prop at 200 RPS, which only produces 1.5 N of thrust. While this is technically sufficient to hover the 300 gram aircraft, it is not sustainable and would lead to motor damage from overheating. It was necessary to change the motor/prop combination.

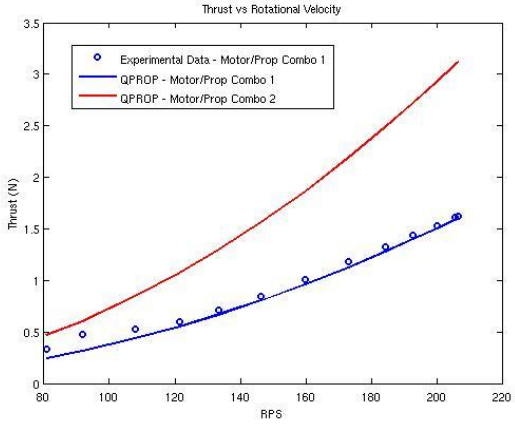

Figure 7. Current consumption vs. rotation speed, experimental data and QPROP.

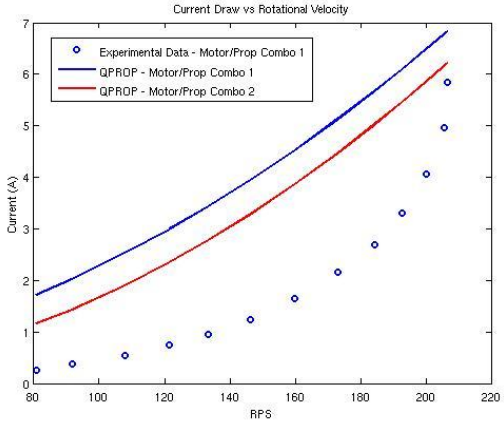

Figure 8. Current consumption vs. rotation speed, experimental data and QPROP.

In order to reduce the required speed of the motors, the diameter of the propeller was increased by 2.5 cm (GWS 6x3x3). Also, a Turnigy 2024-1600 motor was selected with a higher mass, 18 g, to help prevent overheating. The QPROP simulation of the motor/propeller combination is compared with the previous in Figures 6 & 7. The simulation indicates that thrust should increase for a given rotation speed, while current should decrease. Although specific motor testing of the new combination has yet to be performed, in-flight data shows that the new motors and propellers are easily able to maintain vertical flight without overheating. This is due to two effects. The larger propellers produce more thrust at lower rotational speeds, while the higher mass motors are better able to handle the amperage and thus dissipate heat.

V. Aerodynamic Modeling of the MAVion

A generalized aircraft model has been developed to represent the dynamics of the MAVion in both horizontal and vertical flight modes. The effects which generate forces and moments on the aircraft vary as the aircraft transitions between modes. For example, in horizontal flight mode, forces and moments are primarily generated by freestream flow over the wing and control surfaces. However, in vertical mode, when the freestream velocity is zero, forces and moments are entirely generated by the propeller induced velocity flowing down over the body and control surfaces. The aircraft model chosen must represent these two cases, as well as the transition between them.

A. Aircraft Dynamics

Before developing the more complicated interactions between the motors and the aircraft, it is possible to establish equations to describe dynamics regardless of flight mode. To avoid gimbal lock, a singularity in Euler angle representations occurring when a body is pitched by 90 degrees, quaternion methods will be used. A quaternion is composed of four components:

$$\bar{\boldsymbol{\eta}} = \boldsymbol{\eta} + \eta = \eta_1\, i + \eta_2\, j + \eta_3\, k + \eta_4 \qquad 1.$$

The first three components represent the x, y, and z components of a vector in the inertial frame. The body is rotated about this vector. The fourth is a scalar part, and can be used to determine the magnitude of rotation about the vector:

$$\theta_v = 2\cos^{-1}\eta_4 \qquad 2.$$

http://www.imavs.org/

The unit quaternion must satisfy the relationship:

$$\eta_1^2 + \eta_2^2 + \eta_3^2 + \eta_4^2 = 1 \quad (3.)$$

Translational and rotational accelerations in the body frame are described in terms of the quaternion as follows:

$$\begin{aligned} \dot{u} &= rv - qw + 2g(\eta_1\eta_3 - \eta_4\eta_2) + \frac{\sum F_{x_b}}{m} \\ \dot{v} &= -ru + pw + 2g(\eta_2\eta_3 + \eta_4\eta_1) + \frac{\sum F_{y_b}}{m} \\ \dot{w} &= qu - pv + g(\eta_4^2 - \eta_1^2 + \eta_2^2 + \eta_3^2) + \frac{\sum F_{z_b}}{m} \end{aligned} \quad (4.)$$

$$\begin{aligned} \dot{p} &= \frac{J_{xz}(J_{xx} - J_{yy} + J_{zz})}{J_{xx}J_{zz} - J_{xz}^2}pq - \frac{J_{zz}(J_{zz} - J_{yy}) + J_{xz}^2}{J_{xx}J_{zz} - J_{xz}^2}qr + \frac{J_{zz}\sum M_{x_b}}{J_{xx}J_{zz} - J_{xz}^2} + \frac{J_{xz}\sum M_{z_b}}{J_{xx}J_{zz} - J_{xz}^2} \\ \dot{q} &= \frac{(J_{zz} - J_{xx})}{J_{yy}}pr - \frac{J_{xz}}{J_{yy}}(p^2 - r^2) + \frac{\sum M_{y_b}}{J_{yy}} \\ \dot{r} &= \frac{J_{zz}(J_{zz} - J_{yy}) + J_{xz}^2}{J_{xx}J_{zz} - J_{xz}^2}pq - \frac{J_{xz}(J_{xx} - J_{yy} + J_{zz})}{J_{xx}J_{zz} - J_{xz}^2}qr + \frac{J_{xz}\sum M_{x_b}}{J_{xx}J_{zz} - J_{xz}^2} + \frac{J_{zz}\sum M_{z_b}}{J_{xx}J_{zz} - J_{xz}^2} \end{aligned} \quad (5.)$$

Above, *m* is the mass of the aircraft, *Jxx, Jyy, Jzz* are the mass moments of inertia, and $F_x, F_y, F_z, M_x, M_y, M_z$ are forces and moments in the body frame. The rate of change of the quaternion can be represented as:

$$\begin{aligned} \dot{\eta}_1 &= \frac{1}{2}(\eta_4 p - \eta_3 q + \eta_2 r) & \dot{\eta}_3 &= \frac{1}{2}(-\eta_2 p + \eta_1 q + \eta_4 r) \\ \dot{\eta}_2 &= \frac{1}{2}(\eta_3 p + \eta_4 q - \eta_1 r) & \dot{\eta}_4 &= -\frac{1}{2}(\eta_1 p + \eta_2 q + \eta_3 r) \end{aligned} \quad (6.)$$

Position in the inertial frame coordinates (x_i, y_i, z_i) system is determined with the following:

$$\begin{aligned} \dot{x}_i &= u(\eta_4^2 + \eta_1^2 - \eta_2^2 - \eta_3^2) + 2v(\eta_2\eta_1 - \eta_4\eta_3) + 2w(\eta_3\eta_1 + \eta_4\eta_2) \\ \dot{y}_i &= 2u(\eta_2\eta_1 + \eta_4\eta_3) + v(\eta_4^2 - \eta_1^2 + \eta_2^2 - \eta_3^2) + 2w(\eta_3\eta_2 - \eta_4\eta_1) \\ \dot{z}_i &= 2u(\eta_3\eta_1 - \eta_4\eta_2) + 2v(\eta_3\eta_2 + \eta_4\eta_1) + w(\eta_4^2 - \eta_1^2 - \eta_2^2 + \eta_3^2) \end{aligned} \quad (7.)$$

Note that all the above equations apply regardless of the flight mode. It is only left to identify specific forces and moments at each instant. It is convenient to begin with effects generated by the freestream.

B. Freestream Aerodynamic Model

A standard model has been adopted to calculate the forces generated by freestream flow over the wing and control surfaces. It is first necessary to establish the equations for the wind reference variables velocity (V), angle of attack (α), and sideslip (β):

$$\begin{aligned} V &= \sqrt{u^2 + v^2 + w^2} \\ \alpha &= sin^{-1}\left(\frac{w}{u}\right) \\ \beta &= tan^{-1}\left(\frac{v}{V}\right) \end{aligned} \quad (7.)$$

Typically, the lift coefficient is modeled as a linear function of angle of attack, while drag is represented as a quadratic function of either angle of attack or lift. This approach is valid for aircraft which avoid the stall limit. However, for an aircraft performing a transition maneuver, the angle of attack as defined above will reach 90 degrees. Traditional representations of lift, drag, and moment coefficients are only valid below stall. The following equations, based on previous experimental measurements[10], attempt to give a somewhat more generalized picture of the variation of the longitudinal coefficients past the point of stall.

http://www.imavs.org/

$$C_L = C_{L,0} + C_{L,1}\sin\left(\frac{\alpha}{\alpha_{stall}/\frac{\pi}{2}}\right)\cos^2\alpha + C_{L,2}\cos(\alpha)\sin^2\alpha + C_{L,q}\left(\frac{cq}{V}\right) + C_{L,\delta_e}(\delta_e)$$

$$C_D = C_{D,0} + C_{D,1}\sin\alpha + C_{D,2}\sin^2\alpha + C_{D,q}\left(\frac{c|q|}{V}\right) + C_{D,\delta_e}|\delta_e| \qquad 8.$$

$$C_m = C_{m,0} + C_{m,\alpha}(\alpha) + C_{m,q}\left(\frac{cq}{V}\right) + C_{m,\delta_e}(\delta_e)$$

The lift portion of equation 8 has been modeled to mimic the behavior of published data on symmetrical NACA airfoils[11]. The first trigonometric term includes a stall angle, which ensures the peak of the lift occurs at stall, after which the lift coefficient decreases toward zero at 90 degrees. The drag coefficient is shown to increase rapidly for low angle of attack, eventually leveling off to a value which matches drag on a 3D bluff body, typically between 1-2[12]. Figures Figure 12 and Figure 13 show the behavior of these two curves. The moment coefficient equation has a more traditional form. This is simply due to a lack of experimental data showing moment results for high angle of attack. This is unfortunate, since predicting the moment generated on the aircraft during transition is perhaps more important for stability than both lift or drag. It is hoped that future wind-tunnel testing can provided comparison for the above equations.

For the lateral coefficients of sideforce, roll moment, and yaw moment:

$$C_Y = C_{Y,0} + C_{Y,\beta}(\beta) + C_{Y,p}\left(\frac{bp}{2V}\right) + C_{Y,r}\left(\frac{br}{2V}\right) + C_{Y,\delta_e}(\delta_e)$$

$$C_l = C_{l,0} + C_{l,\beta}(\beta) + C_{l,p}\left(\frac{bp}{2V}\right) + C_{l,\delta_e}(\delta_e) \qquad 9.$$

$$C_n = C_{n,0} + C_{n,\beta}(\beta) + C_{n,r}\left(\frac{br}{2V}\right) + C_{n,\delta_e}(\delta_e)$$

In the above equations, c is the average chord and b is the average span. The elevator deflection, δ_e, is given in radians. Although stall is likely to have some effect on the lateral coefficients, again, due to the lack of data available no attempt has been made to develop post-stall versions of these equations.

The resulting freestream forces on the body can then be determined from the coefficients:

$$F_{x_b} = \frac{1}{2}\rho V^2 A\left(-C_D cos(\alpha) + C_L\sin(\alpha)\right) \qquad M_{x_b} = \frac{1}{2}\rho V^2 AbC_l$$

$$F_{Y_b} = \frac{1}{2}\rho V^2 AC_Y \qquad M_{y_b} = \frac{1}{2}\rho V^2 AcC_m \qquad 10.$$

$$F_{z_b} = \frac{1}{2}\rho V^2 A\left(-C_D sin(\alpha) - C_L\cos(\alpha)\right) \qquad M_{z_b} = \frac{1}{2}\rho V^2 AbC_n$$

In the above, A is the area of the flow affected by the freestream, while ρ is the density of air.

The above treatment of freestream effects at high angle of attack is perhaps an oversimplification of stall, but accurately capturing the 3D aerodynamics of stall, particularly in the presence of propeller slipstream, is extremely complex and any analytical model is likely to fall short. There is one consolation, however. High angles of attack will correspond with low freestream velocity. Since the magnitude of forces and moments change with the square of the velocity, these effects will be greatly reduced, especially in comparison with the forces and moments produced by the propulsion and propwash. As one author has proposed, at high angle of attack the freestream effects become second order[13].

C. Propwash Model

As the aircraft transitions from horizontal to vertical flight mode, the forces and moments generated along the wing are increasingly dominated by propwash effects. In horizontal mode, the velocity induced by the propellers is only somewhat greater than the freestream. As the aircraft slows during transition resulting in decreased freestream, the thrust must increase to maintain altitude, thus increasing the propwash velocity.

The following development of propeller-wing interaction follows from McCormick[14]. Momentum theory describes the relationship between static thrust and the static induced velocity (w_0) just behind the propeller:

$$w_0 = \sqrt{\frac{F_{xp,0}}{2\rho\pi R^2}} \qquad 11.$$

http://www.imavs.org/

Here, R is the radius of the propeller. This velocity is then used to evaluate an expression for the velocity in presence of freestream and angle of attack:

$$\left(\frac{w}{w_0}\right)^4 + 2\cos(\alpha)\frac{V}{w_0}\left(\frac{w}{w_0}\right)^3 + \left(\frac{V}{w_0}\right)^2\left(\frac{w}{w_0}\right)^2 = 1 \qquad 12.$$

Although an analytical solution is theoretically available for this quartic equation, it is much simpler to evaluate the four roots numerically. The correct root is real and positive. It is then left to calculate the induced velocity downstream of the propeller, V_h, and the induced angle of attack induced by turning the flow, α_a:

$$V_h = \sqrt{(V + 2w\cos(\alpha))^2 + (2w\sin(\alpha))^2}$$

$$\alpha_s = \sin^{-1}\left(\frac{2w\sin(\alpha)}{V_h}\right) \qquad 13.$$

$$\alpha_a = \alpha - \alpha_s$$

Note that the equation for V_h applies about one diameter downstream of the propeller where the propwash tube diameter and mean velocity are roughly constant.

It is also possible to evaluate the dynamic thrust, neglecting tip losses and profile power. The following relationship is developed by assuming constant induced power, which corresponds to holding a given throttle setting:

$$\frac{F_{xp}}{F_{xp,0}} = \left(\frac{V}{w_0}\cos\alpha + \frac{w}{w_0}\right)^{-1} \qquad 14.$$

Just to serve as an example By applying the propeller-momentum theory and the continuity equation it is possible to predict the diameter of the stream tubes over the wing[2]:

$$r(s) = \sqrt{\frac{w(s)R^2}{w(0)}} \qquad 15.$$

In the above equations, s is the distance from the propeller along the chord, T is the propeller thrust, R is the propeller radius, and V is the freestream velocity. For visualization, Figure 9 & Figure 10 have been attached showing predicted stream tube size for horizontal and vertical flight, respectively.

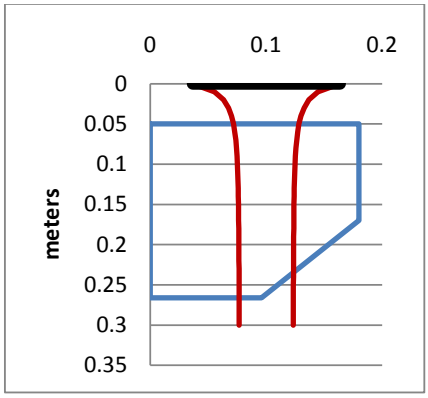

Figure 9. Stream tube prediction corresponding to horizontal flight.

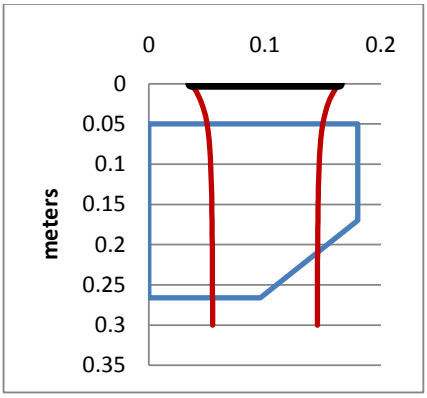

Figure 10. Stream tube prediction corresponding to vertical flight

Figure 9 shows horizontal flight, with V=10m/s and producing 0.3N thrust. Figure 10 corresponds to hover, with zero freestream and 2 N of thrust. The percentage of the wing immersed in the slipstream in vertical flight is significantly greater than for the horizontal case. This is fortunate, as the increased slipstream size and velocity improves control effects in hover. Also note that for both cases the streamtube radius is nearly constant at roughly one half diameter behind the propeller.

Knowing the velocity of the induced flow over the surface of the wing, it is possible to recalculate the aerodynamic coefficients based on V_h and α_a, rather than their freestream counterparts. These streamtube coefficients are used to calculate forces and moments developed along the portion of the wing covered by the

http://www.imavs.org/

streamtubes, as calculated by Equations 14. The forces and moments generated by the freestream and streamtubes are then totaled for each wing, and applied to the center of gravity of the aircraft.

There are several effects not captured by the above assumption that the same coefficients apply to both freestream and slipstream, and forces and moments are simply calculated for the two separate regions and summed. First, the thrust from the propellers may be turned downward by the control surfaces resulting in an increased lift contribution. Additionally, the circulation about the wing is increased as the turning slipstream acts as a jet flap on the flow external to the stream. Finally, the swirl of the propwash can produce a beneficial effect on the lift of the aircraft, by cancelling in part the pressure gradients which give rise to wingtip vortices. In one study, this effect was found to increase the lift coefficient by as much as 10%. Correction factors can be added to the lift coefficient to capture these effects, but with a lack of experimental data to verify the magnitude of effect, their addition is not justified here.

D. Determination of Aerodynamic Coefficients

As a preliminary method of determining aerodynamic coefficients, an analysis tool for low Reynold's numbers called XFLR5 has been used[15]. This program makes use of the already mentioned XFOIL to calculate 2D airfoil coefficients, then applies lifiting line, vortex-lattice, or 3D panel methods to determine 3D wing characteristics. These methods are currently limited to calculations below stall, so all data fitting is performed up to 30 degrees angle of attack.

A model of the MAVion has been generated in XFLR5, and results calculated for a range of velocities and angles of attack.

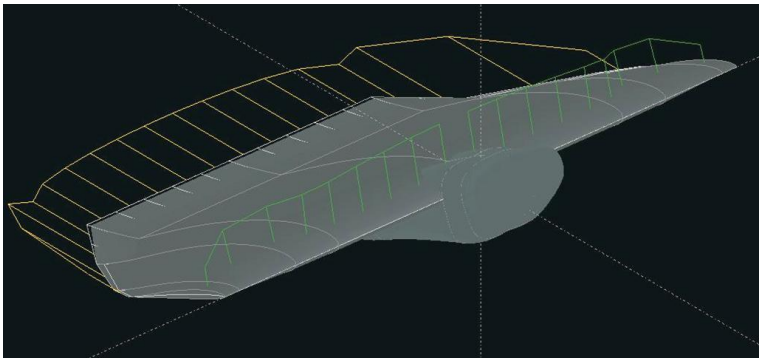

Figure 11. XFLR5 Screenshot showing sample lift and drag profiles over the MAVion

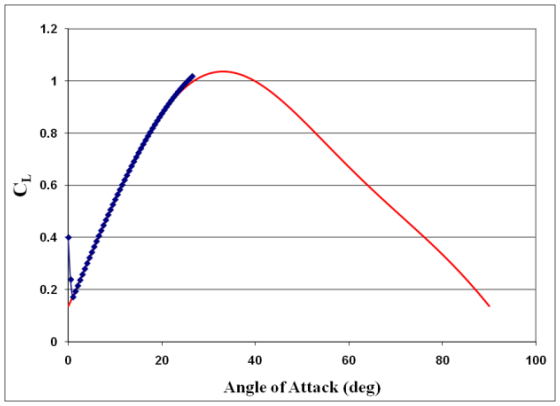

Figure 12. Lift profile, elevator deflected down 5 degrees. Blue profile generated by XFLR5, red from model equation 8.

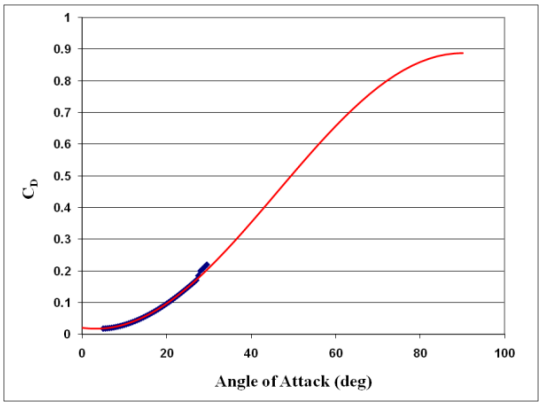

Figure 13. Drag Profile, elevator deflected up 10 degrees. Blue profile generated by XFLR5, red from model equation 8.

http://www.imavs.org/

The data from XFLR5 has been used to generate lift, drag, and moment polars up to 30 degrees angle of attack for flap angles between -20 and +20 degrees. This data was used to find coefficients for equation set 8. The coefficients found are shown in the table below.

C_{L0}	0.043	C_{D0}	0.017	C_{m0}	-0.011
C_{L1}	0.796	C_{D1}	-0.026	$C_{m\alpha}$	-0.139
C_{L2}	1.58	C_{D2}	1.06	$C_{m\delta}$	-0.01
$C_{L\delta}$	0.017	$C_{D\delta}$	0.104		

While XFLR5 has been useful to predict freestream coefficients for below stall angles of attack, it is desirable to simulate effects of propwash impingement on the wing for a greater range of angle of attack. This may be done using a higher-fidelity CFD package, such as FLUENT[16]. This is well known CFD software with very broad capabilities, from 3D meshing to turbulence modeling. It is also possible to implement a fan boundary condition with pressure jump and swirl effects to simulate a propeller.

In order to compare the results from XFLR5 in combination with the aerodynamic model of propeller flow impingement on the wing, some preliminary work has been performed using FLUENT. An image of a grid generated for the MAVion is presented in Figure 14.

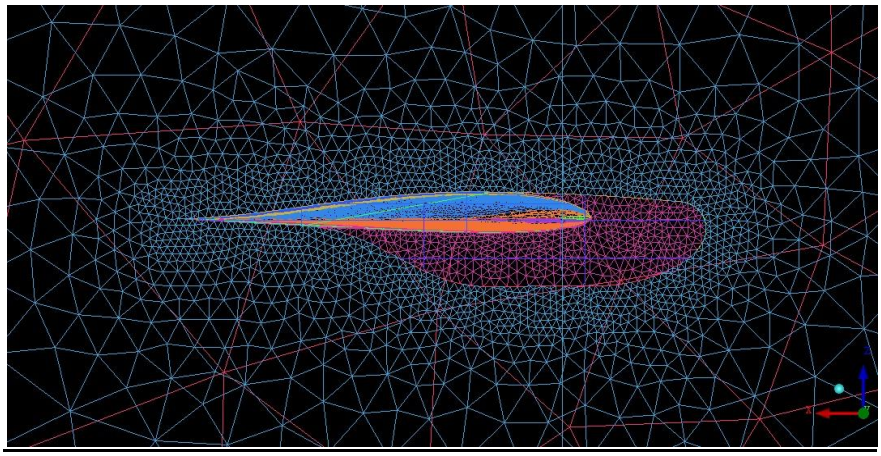

Figure 14. Grid generated using FLUENT for the MAVion.

A single case has been generated thus far, corresponding to freestream V= 15 m/s at zero degrees angle of attack. The propellers are modeled as a pressure drop, with the pressure change across the propellers corresponding to 1 N of thrust. Velocity swirl may also be added to the propeller output. As indicated, this work is preliminary, and no attempt has yet been made to validate or compare the data generated using FLUENT. Additionally, no attempt has been made to determine lateral coefficients. Once FLUENT results have been appropriate validated, lateral behavior of the MAVion can also be studied, including propeller swirl. However, these simulations should only serve as preliminaries to a full wind-tunnel campaign, which will be performed in the near future. During this experimental testing, the aerodynamic model presented in this paper will be tested for suitability, particularly the lift and drag curves, as well as the propeller-wing interaction model.

http://www.imavs.org/

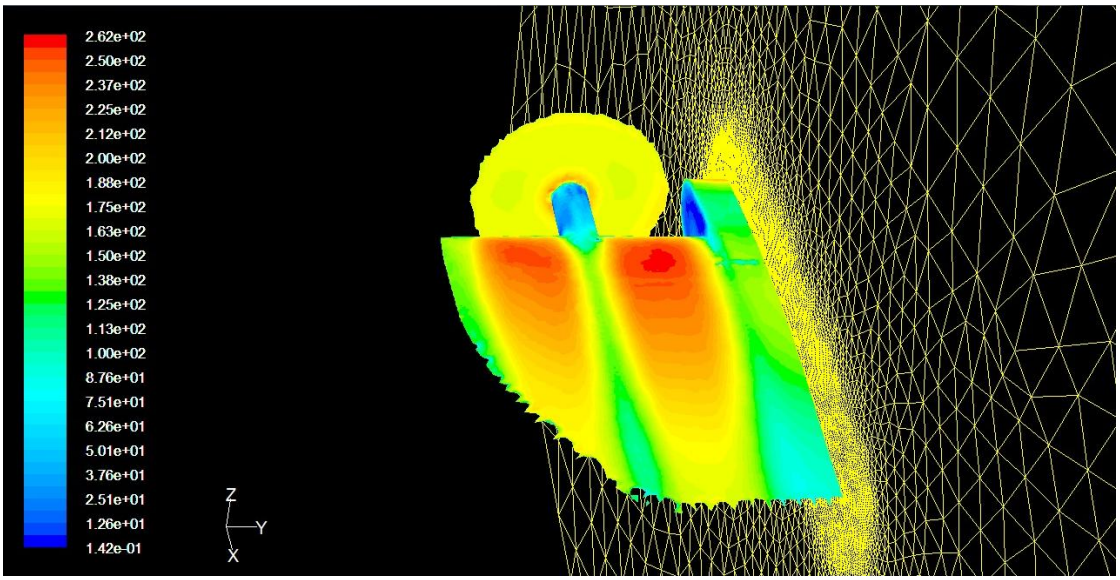

Figure 15. FLUENT pressure contours (Pa) showing effect of 1 N thrust propeller, no swirl. V=15 m/s.

E. 6 DOF Flight Simulator

The aerodynamic model presented above has been implemented into a 6 degree of freedom flight simulator. Equations 4-7 are resolved using 4 step Runge-Kutta integration. Full state information from the plant is received by an estimation block which simulates gyros, accelerometers, and GPS measurements. The estimated aircraft state is then received by the controller, which outputs commands to the actuators. These are modelled as first order equations with time constants, and the results are then re-fed into the plant. A simplified diagram of the simulator is shown in Figure 16.

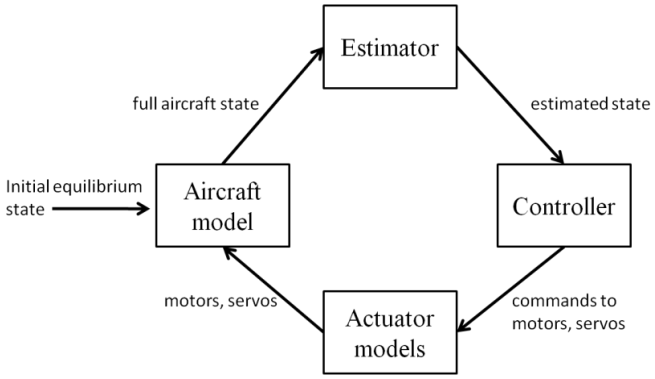

Figure 16. Simplified diagram of flight simulator.

The results from the simulator are not regarded as being in any way indicative of actual aircraft performance. However, it is a very useful tool for preliminary control design and code development. The PID controllers presented later in this paper were first tested on the simulator. Higher level guidance and navigation schemes have also been tested on the simulator, and will be hardware tested on the MAVion as the move is made to horizontal and transition flights.

VI. Automatic Control of the MAVion

The original purpose of the MAVion, as stated in the introduction section of this document, is to provide an aircraft which will switch between horizontal and vertical flight modes to fulfill a complex mission. While much

http://www.imavs.org/

work has been done to properly design and fabricate the platform itself to enable the transition, the bulk of performing the maneuver must rest on the automatic controller. The controller must be general enough to be used in both modes, yet provide precise navigation and stability. It is preferable to find a solution that does not require a large structural change when performing the transition. One technique that can help smooth the transition between the two modes is the exclusive use of quaternions, thus avoiding discontinuities present in Euler based controllers. Gain scheduling, online parameter estimation, and adaptive control are also promising possibilities, although beyond the present scope of the paper. While only the vertical controller will be presented here, it is meant to be generalized for both modes.

A. Autopilot Hardware

As mentioned previously, a new autopilot system has been implemented into the vertical version of the MAVion. The components of the system, developed by the Mathematics, Information, and Controls Department at ISAE, are described here in detail:

Board

The board has been custom built to include a ARM7 processor, ports for ADC, I2C communication with the speed controllers, modem, PWM to the servos, external GPS, and IMU.

Figure 17. Autopilot board and modem.

Modem

The well known XBee 802.15.4 OEM RF Module[17] is used at 2.4 GHz with 1mW power. The indicated indoor line-of-site range is 30 meters.

IMU

The SBG Systems IG-500N GPS aided Automatic Heading and Reference System[18] runs an Extended Kalman Filter to combine gyroscopes, accelerometers, temperature, pressure, and magnetometer readings to produce attitude information at 100Hz. Inclusion of GPS measurements allows position information.

Figure 18. SBG IG-500N IMU

Electronic Speed Controller

The Mikrokopter BL-Ctrl v1.1[19] is typically used for quadrotors. It communicates via I2C and provides very quick response times (<20 ms).

Figure 19. Mikrokopter BL-Ctrl v1.1

B. Quaternion Based Attitude Hold

To avoid the possibility of gimbal lock the MAVion controller relies solely on quaternion representations of angular rotations. Again, the quaternion is composed of a single scalar component and three vector components that represent the axis about which a body is rotated. It is necessary to use two principles of quaternion mathematics to develop the controller. First, the rotation of a vector, x1, to another reference frame, x2, can be described using the quaternion as follows:

$$\boldsymbol{x_2 = \bar{\eta} x_1 \bar{\eta}^{-1}} \qquad 16.$$

This process is called conjugation. To invert the quaternion in the equation above, simply switch the sign of the vector components and normalize by the magnitude.

Second, the rotations of two quaternions can be combined using composition6:

http://www.imavs.org/

$$\bar{\eta}'' = \bar{\eta}' \otimes \bar{\eta} = \{\bar{\eta}\}\bar{\eta}'$$
$$\{\bar{\eta}\} = \begin{bmatrix} \eta_4 & -\eta_3 & \eta_2 & \eta_1 \\ \eta_3 & \eta_4 & -\eta_1 & \eta_2 \\ -\eta_2 & \eta_1 & \eta_4 & \eta_3 \\ -\eta_1 & -\eta_2 & -\eta_3 & \eta_4 \end{bmatrix} \quad 17.$$

Typically, a desired orientation is supplied to the controller by a navigation routine. For the case of purely vertical flight, this desired quaternion can be expressed as a composition of two rotations. Beginning with the aircraft oriented with the inertial North-East-Down (NED) coordinates, with the nose pointed north and the right wing pointing east, the first rotation points the nose straight up along the negative z NED axis, with the belly of the aircraft pointing along the x NED axis. Based on equations 2 & 3, this is simply:

$$\bar{\eta}_v = \begin{bmatrix} 0 \\ \sin\frac{\pi}{4} \\ 0 \\ \cos\frac{\pi}{4} \end{bmatrix} \quad 18.$$

If it is desired to point the belly (heading) of the aircraft in any other direction, *h* radians from north, one simply needs to apply a rotation about the body *x* axis, which can be done by composing $\boldsymbol{\eta_v}$ with the following:

$$\bar{\eta}_h = \begin{bmatrix} \sin\frac{h}{2} \\ 0 \\ 0 \\ \cos\frac{h}{2} \end{bmatrix} \quad 19.$$

The result will be a desired quaternion, $\boldsymbol{\eta_d}$, which the aircraft controller will try to maintain. Any deviation from this desired quaternion will result in an error. The error can be expressed again using the composition operation. Writing the actual aircraft attitude by $\boldsymbol{\eta_a}$, the error between the current and the desired quaternion can be written using equation 17:

$$\bar{\eta}_d = \bar{\eta}_e \otimes \bar{\eta}_a$$
$$\bar{\eta}_e = \{\bar{\eta}_a\}\bar{\eta}_d \quad 20.$$

Note that this error quaternion, based in the body reference frame of the aircraft, represents the rotation that the aircraft must undergo to achieve the desired orientation. From this it follows that one must simply control rotation about the body x, y, and z axes. For convenience, these are called aileron, elevator, and rudder operations. A simple PD controller has been implemented with feedback loops for each of these three. A PD controller attempts to correct proportional and derivative errors in the signal by feedback. Proportional error for each loop is simply the vector value of $\boldsymbol{\eta_e}$, corresponding to the axis of rotation required, while the derivative error is defined as the desired rotational velocity minus the actual rotational velocity measured from the gyroscopes on the IMU. Equations for the three loops require six total gains to be tuned:

$$aileron = K_{p,a}(\eta_{e,1}) + K_{d,a}(p_m - p_a)$$
$$elevator = K_{p,e}(\eta_{e,2}) + K_{d,e}(q_m - q_a) \quad 21.$$
$$rudder = K_{p,r}(\eta_{e,3}) + K_{d,r}(r_m - r_a)$$

Often, the desired rotational velocity is simply zero. Instead, here a reference model is used to produce idealized proportional and rotational responses to desired orientation. The error quaternion is then based not on the desired quaternion, but the proportional response of the reference model. The model rotational velocity is used as the desired velocity in equation 21. This essentially causes the aircraft to try to track the behavior of the idealized model, rather than to feed it commands directly. The reference model may be considered as a filter to the navigational commands, ensuring they are always reasonable. The reference model rotational velocities, $\boldsymbol{\omega_m}$ are defined as second order:

$$\dot{\boldsymbol{\omega}}_{\boldsymbol{m}} + 2\varpi_n \boldsymbol{\zeta} \boldsymbol{\omega_m} = \varpi_n^2 \boldsymbol{\eta_{e,m}} \quad 22.$$

http://www.imavs.org/

Here, the natural frequency, ω_n and the damping ratio, ζ are tuned to give ideal performance of the aircraft. The term $\boldsymbol{\eta_{e,m}}$ is the error between $\boldsymbol{\eta_d}$ and the model quaternion, $\boldsymbol{\eta_m}$, which is calculated as follows:

$$\dot{\boldsymbol{\eta}}_{\boldsymbol{m}} = \frac{1}{2}\begin{pmatrix} \eta_4\varpi_{m,1} - \eta_3\varpi_{m,2} + \eta_2\varpi_{m,3} \\ \eta_3\varpi_{m,1} + \eta_4\varpi_{m,2} - \eta_1\varpi_{m,3} \\ -\eta_2\varpi_{m,1} + \eta_1\varpi_{m,2} + \eta_4\varpi_{m,3} \\ -\eta_1\varpi_{m,1} - \eta_2\varpi_{m,2} - \eta_3\varpi_{m,3} \end{pmatrix} \quad 23.$$

Then, the error quaternion used in equation 20 is defined between the reference model quaternion and the actual quaternion. The desired rotational velocity is the model reference rotational velocity. A diagram of this overall controller is given in Figure 20.

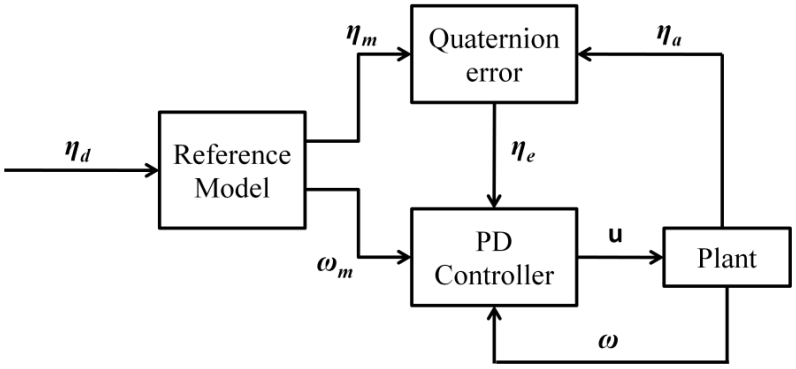

Figure 20. Diagram of Model Reference Quaternion PD controller

C. Altitude Hold Autopilot

A LV-MaxSonar – EZ1 Sonar range finder from Maxbotix[20] has been installed on the aircraft to give altitude readings. The returned result, after calibration, is not actually the altitude of the aircraft, but the position from the tail of the aircraft to the ground along the negative body x axis. This means that any rotations of the body away from vertical result in a change in sensor reading. The sensor reading can be transformed into altitude, or the negative NED z axis, by applying the vector transformation listed in equation 16. Since the actual aircraft quaternion represents a rotation from NED to body, it is necessary to use the inverse, which is the rotation from body to NED. Figure 21 displays the concept of rotation graphically. Equation 24 shows how altitude is calculated from the sensor reading.

A PID control loop, much like equation 21, uses the measurement to maintain altitude. The rate and integral errors are calculated as numerical derivative and integrals, respectively. The rate information must be filtered before use, as calculating a derivative adds significant noise to the signal. This introduces some lag into the measurement, but not enough to be detrimental to the performance of the altitude hold loop.

$$altitude = -2(\eta_1\eta_3 - \eta_2\eta_4)\left(d_{sensor} + c - x_{cg}\right) \quad 24.$$

http://www.imavs.org/

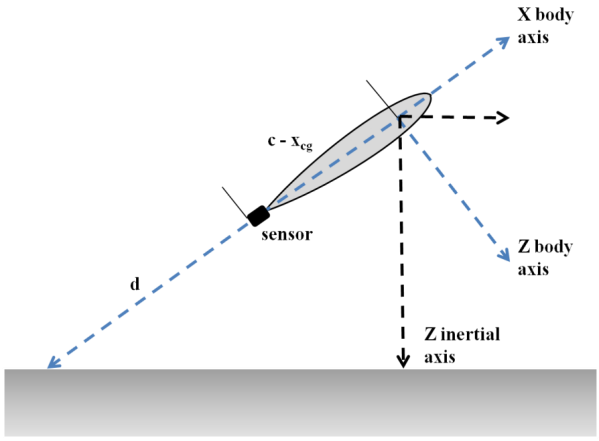

Figure 21. Diagram of rotation necessary to read altitude from ultrasonic range finder.

D. Servo and Motor Mixing

Although the MAVion has elevons and no rudder, the same effects can be attained by simply transforming these three operations into the separate servo and motor commands. This is called mixing in the hobby aircraft industry. Mixing is performed with the following equations to output servo PWM values between 1000-2000 μs, and throttle values for each motor between 0-100%. Elevator, aileron, and rudder commands are given between -1 and +1, while the throttle command is between zero and one hundred.

$$Servo\ 1 = 500(elevator - aileron) + 1500$$
$$Servo\ 2 = 500(elevator + aileron) + 1500$$
$$Motor\ 1 = throttle - rudder * 50$$
$$Motor\ 2 = throttle + rudder * 50 \quad (25.)$$

E. Attitude Control Bench Testing

To validate the orientation control approach described above, 3 separate bench tests were performed for each axis of rotation. A sturdy version of the aircraft, constructed of fiberglass, was mounted onto a test stand. Pins were inserted to isolate the pitch, roll, and yaw degrees of freedom. Photos of the test apparatus for pitch and yaw are shown below.

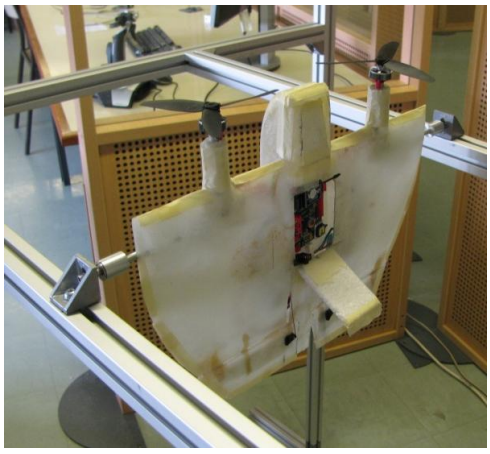

Figure 22. MAVion test bench model in pitch control configuration.

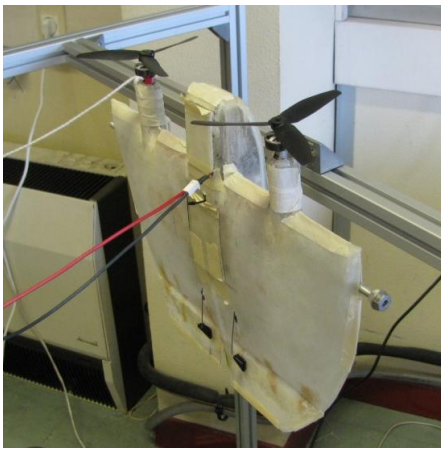

Figure 23. MAVion test bench model in yaw control configuration.

http://www.imavs.org/

http://www.imavs.org/

For the vertical MAVion, roll provides the heading, while pitch and yaw are used to stabilize the aircraft. The pitch and yaw tests especially were key in determining the proper gains and validating the control code before flight testing was begun.

F. Flight Testing

After successful validation of the attitude control loops, flight testing was begun indoors. The gains found while bench testing were applied to the flight version of the aircraft. Control inputs from a joystick were also added to allow a pilot to control position of the aircraft by actuating the control surfaces and motors. After a few trials to determine proper control surface trim, the aircraft was able to hover with very little correction from the manual pilot. The altitude loops were then applied, and satisfactory gains were found by trial and error. Flights thus far have been limited to less than three minutes in length, although the maximum flight time with a 1000mAh LiPo battery is expected to be around 5 minutes. An image of the aircraft in flight is given in Figure 24.

Figure 24. The MAVion in vertical flight mode.

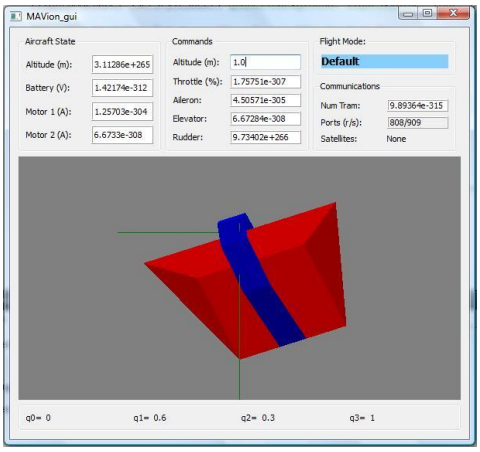

Figure 25. MAVion graphical user interface

A graphical user interface has been developed using Qt[21] and OpenGL to display flight information such as altitude, battery voltage, motor current, flight mode, and current aircraft orientation. A screenshot of the interface is given in Figure 25.

A state machine was implemented into the flight version in order to ensure safety of the operator and aircraft, to properly test the aircraft before each flight, and to separate the different functional modes. The number and complexity of modes will continue to grow as the functionality of the MAVion increases. A diagram of the state machine is presented in Figure 26.

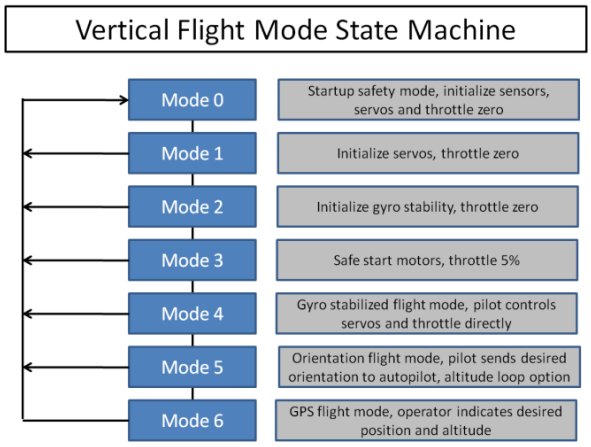

Figure 26. MAVion state machine.

VII. Conclusion

A variety of tools have been used to design, build, and test an aircraft capable of performing both vertical and horizontal flight modes. A general aerodynamic model of the MAVion has been developed to understand the behavior of the aircraft during the transition between these two modes. This understanding aided in the development of a model-referenced PD controller to maintain a desired quaternion based orientation. The current version of the MAVion has been demonstrated in stable vertical flight, while previous versions have been used in horizontal mode. The next step in the progression of the MAVion project is to perform the transition between the two modes. The MAVion is a relatively simple aircraft which will provide a single solution for a complicated, multi-faceted mission.

VIII. Acknowledgements

The authors wish to thank the Air Force Research Laboratory European Office of Research and Development for generously funding this research. Additional appreciation is expressed to the many technicians in the composite, propulsion, and controls labs at ISAE who have aided in the development of the MAVion. Alix, Etienne, Flavien, and Guillaume provided critical manpower and support throughout the entirety of the project. Final thanks go to Dominique Bernard for his expert advice and magnificent pilot skills.

---

[1] Allen, Francis J. (2007). "Bolt upright - Convair's and Lockheed's VTOL fighters". Air Enthusiast (Key Publishing) January/February 2007 (127): 13-20. ISSN 0143-5450.
[2] Shkarayev, S., Bataille, B., Moschetta, J.M., "Aerodynamic Design of VTOL Micro Air Vehicles", 3rd US-European Competition and Workshop on Micro Air Vehicle Systems & European Micro Air Vehicle Conference and Flight Competition, Toulouse, France, September 2007.
[3] Frank, A., McGrew, J.S., Valenti, M., Levine, D., How, J.P., "Hover, Transition, and Level Flight Control Design for a Single-Propeller Indoor Airplane", Guidance, Navigation, and Controls Conference, Aug 2007.
[4] The MLB Company, "VBAT UAV Brochure", http://www.spyplanes.com.
[5] Stone, H., Wong, K.C. "Preliminary Design of a Tandem-Wing Tail-Sitter UAV Using Multi-Disciplinary Design Optimisation ", International Aerospace Congress, Sydney, February 1997, p707-720.
[6] Knoebel, N.B., McLain, T.W., "Adaptive Quaternion Control of a Miniature Tailsitter UAV". 2008 American Control Conference, Seattle, June 2008.
[7] Poinsot, D., Piquereau, A., Caroline, B., "Fixed wings MAV controlled by deflection of airflow in a hover flight phase", European Micro Air Vehicles Conference, 2006.
[8] http://paparazzi.enac.fr/wiki/Main_Page
[9] http://web.mit.edu/drela/Public/web/qprop/
[10] Bataille, B. "VERTIGO aerodynamic and propulsion anaylsis". Internal Report. ISAE, Toulouse, France, February 2008
[11] Sheldahl, R.E. , Klimas, P.C., "Aerodynamic Characteristics of Seven Symmetrical Airfoil Sections Through 180-Degree Angle of Attack For Use In Aerodynamic Analysis of Vertical Axis Wind Turbines", Sandia National Laboratories Wind Power Technoloies Online Reports SAND80-2114, http://windpower.sandia.gov/topical.htm
[12] Munson, B.R., Young, D.F., Theodore, H.O., "Fundamentals of Fluid Mechanics", 4th Edition, John Wiley & Sons, Inc,, 2002.
[13] Stone, R., Clark, G., "Optimization of Transition Manoeuvres for a Tail-Sitter Unmanned Air Vehicle (UAV)", http://www.aeromech.usyd.edu.au/uav/twing/
[14] McCormick, B. W. Jr., Aerodynamics of V/STOL Flight, Dover Publications, Inc., Mineola, NY, 1999
[15] http://xflr5.sourceforge.net/xflr5.htm
[16] http://www.fluent.com
[17] http://www.digi.com/products/wireless/point-multipoint/xbee-series1-module.jsp#overview
[18] http://www.sbg-systems.com/products/ig-500n
[19] http://www.mikrokopter.de/ucwiki/en/BL-Ctrl_V1_1
[20] http://www.maxbotix.com/uploads/LV-MaxSonar-EZ1-Datasheet.pdf
[21] http://qt.nokia.com/products/

http://www.imavs.org/